Giant charge inversion of a macroion due to multivalent counterions and monovalent coions: Molecular dynamics study

Motohiko Tanaka
National Institute for Fusion Science, Toki 509-5292, Japan

A. Yu Grosberg
Department of Physics, University of Minnesota, Minneapolis, Minnesota 55455

(Received 14 February 2001; accepted 12 April 2001)

We report molecular dynamics simulation of the (overall neutral) system consisting of an immobile macroion surrounded by the electrolyte of multivalent counterions and monovalent coions. In a short time ($<$ a few nanoseconds), counterions adsorb on the macroion surface in the amount much exceeding neutralization requirement, thus effectively inverting the sign of the macroion charge. We find two conditions necessary for charge inversion, namely, counterions must be multivalently charged and Coulomb interactions must be strong enough compared to thermal energy. On the other hand, coion condensation on the multivalent counterions similar to Bjerrum pairing is the major factor restricting the amount of charge inversion. Depending on parameters, we observe inverted charge up to about 200% the original charge of the macroion in absolute value. The inverted charge scales as $\sim\zeta^{1/2}$ when $\zeta<1$ and crosses over to $\sim\zeta$ for $\zeta>1$, where $\zeta=(A_0/r_s)^2$, r_s is the Debye screening length in the electrolyte and A_0 is the distance between adsorbed counterions under neutralizing conditions. These findings are consistent with the theory of ''giant charge inversion'' [Phys. Rev. Lett. **85**, 1568 (2000)]. © *2001 American Institute of Physics.*
[DOI: 10.1063/1.1377033]

I. INTRODUCTION

Correlation effects in the systems of charged particles, such as plasma or electrolyte solution, are well known since the works by Debye and Hückel in 1923.[1] Classical intuition suggests that correlation can be viewed as screening in which a cloud of ions around, say, positive particle is slightly dominated by negative counterions, such that for an outside observer (who measures the electric field) the shield of predominantly negative charges effectively reduces the central positive charge. Recently, a significant attention has been attracted by the notion that much more dramatic effect is possible in the system with strongly charged ions.[2] Namely, instead of charge reduction due to the shielding, it is possible to observe charge inversion due to the ''overscreening.'' Furthermore, it was shown that the inverted charge may be quite large, even larger in absolute value than the original bare charge, giving rise to the concept of ''giant'' charge inversion.[3]

In the present paper, we use molecular dynamics simulation technique to address the question of possible limits of charge inversion. Overall, we confirm the theoretical prediction[3] and observe ''giant'' charge inversion, with the ratio of inverted and bare charges reaching up to about two (in absolute value).

Although we consider here only primitive schematic model with spherical ions immersed in the medium of a constant dielectric permeability ϵ, this should be viewed as the step towards better understanding of such first magnitude scientific problems as, e.g., that of chromatin structure. Indeed, chromatin represents a complex of strongly negatively charged thread of DNA with positively charged smaller protein molecules. For instance, virtually every paper on charge inversion mentions the fact that protein core of a nucleosome particle[4] carries lesser amount of positive charge than the amount of negative charge on the wrapped around DNA. On a simpler level, complexes of polycations and polyanyons were under scrutiny for a long time,[5] as well as complexes of charged polymers with charged colloids.[6]

In theoretical aspect, the most advanced treatment of charge inversion is due to Shklovskii and his coworkers.[2,3,7,8] In these works, the universal physical mechanism behind charge inversion is recognized as correlations between shielding ions (see also brief review paper[9]). It was emphasized[2] that the idealized image of these shielding counterions form a Wigner crystal on the surface of the shielded macroion (see also earlier work[10]). However, it was mentioned[2] and addressed in more detail[7,8] that in most real cases, correlations are not quite as strong as to produce a crystal, but sufficient to maintain short range order, and, therefore, correlation energy is similar to that of a crystal. Obviously, this mechanism is operational when shielding ions are strongly charged. Furthermore, it was realized that the best situation for charge inversion occurs when monovalent salt is present in addition to strongly charged ions.[3,11] Salt ions, as their charges are small, behave in a ''traditional'' way; they simply screen all interactions at the distance about Debye length r_s. However trivial itself, this leads to a dramatic increase in charge inversion, because the attraction of a counterion to its Wigner–Seitz cell on the macroion surface is over a significantly shorter range than the repulsion of a counterion from the uncompensated charge of all other counterions. For completeness, we mention here

also recent works developing charge inversion theory to include polyelectrolyte ions,[12–14] alternative approach treating correlations in a different manner,[15] as well as more formal theoretical approaches.[16]

Numerical studies of charge inversion were made by several authors, starting from the pioneering works.[17,18] In one of the papers,[18] charge reversal of charged planar walls was studied for the case of multivalent counterions and salt, and polyelectrolyte chains. In recent works[19–21] computer simulations were reported along with various ways to rederive and re-examine the concept of lateral correlations between counterions as the driving force behind charge inversion. These papers[19,20] reported impressive agreement between theoretical conjectures and their computational results. However sophisticated, these simulations except one brief report[18] concentrated on the cases of no added salt and of abundance of counterions. In other words, people mostly examined the very dilute extreme cases with respect to macroions assuming at the same time finite concentration of counterions. Our first intent in the present work is to relax this serious restriction and to simulate a realistic model in which thermodynamic cost of adsorption of counterions on the surface of a macroion is contributed by both the events on the macroion surface and in the surrounding solution.

The other closely connected goal of our present study has to do with the following delicate aspect of the ''giant'' charge inversion scenario. In order to make correlations and charge inversion stronger, one is tempted to choose larger ratio of the Coulomb energy to thermal energy. But when it is too large, the small salt ions start to condense on the surfaces of counterions, effectively reducing their charge. Therefore, charge inversion is expected to be the strongest in the intermediate regime when correlations between counterions are already strong but condensation of small ions on them is still weak. Therefore, we want to check computationally in the present work how robust is this theoretical prediction.

To achieve the above stated goals, we perform molecular dynamics study of the system consisting of a single macroion, large number of multivalent counterions, and a multitude of monovalent coions immersed in a Langevin fluid. We note that hydrodynamic effects, which may be important for interactions between colloidal particles away from thermodynamic equilibrium,[22–24] are ignored in the present study, because we concentrate on the equilibrium aspects only.

The paper is organized as follows. The simulation method and parameters are described in Sec. II. In Sec. III, by direct measurement of the peak height of the radial charge distribution we show that the ''giant'' charge inversion takes place when the following two conditions are simultaneously met: (1) multivalent counterions with valence $Z \geqslant 2$ are present, and (2) Coulomb energy prevails over the thermal energy at the length scale of a single ion size, a: $\Gamma_a = Ze^2/\epsilon a k_B T > 1$. We study in details the dependence of charge inversion on the radius and charge of the macroion, the valence and density of counterions and coions, and temperature. For large density and valence of counterions, the amount of inverted charge increases linearly with ionic strength, and reaches up to 200% the original macroion charge.

Extension of the present work to the case under electrophoretic environments is discussed in a separate paper[25] in which the effect of an applied electric field on the charge inversion process is investigated with the use of molecular dynamics simulation.

II. SIMULATION METHOD AND PARAMETERS

A. Equations

Specifically, we consider the following model. The system includes a single macroion with negative charge $Q_0 < 0$, N^+ multivalent counterions with a positive charge Ze each, and N^- monovalent coions with a negative charge $(-e)$ each ($e>0$ is the elementary charge). Overall charge neutrality is strictly enforced: $Q_0 + ZeN^+ - eN^- = 0$. All ions are confined within the three-dimensional simulation domain having spherical shape with radius R_M. The macroion is considered immobile; it is placed at the origin (center of the domain), and all other ions are mobile. All ions are supposed to be of spherical shapes, with macroion having radius R_0 and all mobile ions having identical radius a; a serves also as a unit of length.

The molecular dynamics simulation here solves the Newton–Langevin equations of motion,

$$m\frac{d\mathbf{v}_i}{dt} = -\nabla\Phi(\mathbf{r}_i) - \nabla\phi(\mathbf{r}_i) - \nu a\mathbf{v}_i + \mathbf{F}_{\mathrm{th}},$$
$$\frac{d\mathbf{r}_i}{dt} = \mathbf{v}_i, \tag{1}$$

where the potentials Φ and ϕ, describe interactions of a given ion with other mobile ions and with the macroion, respectively,

$$\Phi(\mathbf{r}_i) = \sum_j \left\{ \frac{Z_i Z_j e^2}{\epsilon r_{ij}} + \epsilon_{\mathrm{LJ}} \left(\left(\frac{a}{r_{ij}}\right)^{12} - \left(\frac{a}{r_{ij}}\right)^{6} \right) \right\},$$
$$\phi(\mathbf{r}_i) = Z_i e \frac{Q_0}{\epsilon r_i}. \tag{2}$$

Here, $\mathbf{r}_i$ and $\mathbf{v}_i$ are the position and velocity vectors of the ith particle, $r_{ij} = |\mathbf{r}_i - \mathbf{r}_j|$, ϵ is the dielectric constant, ϵ_{LJ} is the Lennard-Jones energy. As for the boundaries, we assume elastic reflection every time when a mobile ion hits either the domain boundary at $r = R_M$ or the macroion surface at $r = R_0$. The last two terms of Eq. (1) represent the Langevin thermostat due to the surrounding neutral medium. The Stokes formula for a sphere is adopted for the friction term with ν being the friction constant, and $\mathbf{F}_{\mathrm{th}}$ is the random δ-correlated thermal agitation. Since we are interested in the static (equilibrium) configurations where the macroion is at rest, we assume that the thermal agitation force $f_i(t)$ does not depend on time, and that it satisfies $\langle f_i(t) f_i(t') \rangle = 2\pi\nu a\,\delta(t-t')$.

The inertia term is retained in the momentum equation for numerical stability of the electrostatic forces; masses of all mobile ions are assumed identical, equal to m. This leads

to the choice of ω_p^{-1} as the natural time unit, where $\omega_p = (4\pi n_0 e^2/\epsilon m)^{1/2}$ is plasma frequency and n_0 the average ion number density.

B. Parameters

It must be born in mind that phenomena resembling charge inversion may occur when other forces, apart from Coulomb electrostatic ones, operate in the system (including complicated helical shape of the molecules involved[26]). In this study we are interested in the situation when pure electrostatic forces dominate. Accordingly, we choose $\epsilon_{\mathrm{LJ}} = (1/12)e^2/\epsilon a$; this corresponds to the depth of Lennard-Jones potential well equal to $-\epsilon_{\mathrm{LJ}}/4 = -(1/48)e^2/\epsilon a$, which means that the Lennard-Jones attraction force is very small compared to the Coulomb force even for monovalent ions at the distance of the ion size a.

We also consider densities at which short range repulsion (excluded volume effect) between ions is not important, as volume fraction of particles in the simulation domain, $\phi = \phi^+ + \phi^- = a^3(N^+ + N^-)/(R_M^3 - R_0^3)$, is small, about $\phi \approx 0.05$ or less for all cases considered in this paper.

By contrast, Coulomb interactions are strong. To be more specific, there are several relevant parameters controlling different manifestations of Coulomb forces. First of all, multivalent Z ions are attracted to the macroion and can be adsorbed on its surface. This is controlled by the parameter

$$\Gamma_Q = \frac{ZeQ_0}{\epsilon R_0 T} \tag{3}$$

(for the temperature T, we use energy units and omit Boltzmann constant k_B). Second, monovalent coions are attracted to the multivalent counterions (Z ions) and condense there, which is controlled by the parameter

$$\Gamma_a = \frac{Ze^2}{\epsilon a T}. \tag{4}$$

A little more delicate matter is the possible correlation between repelling ions, particularly those adsorbed on the macroion. This is characterized by $\Gamma = Z^2 e^2/\epsilon A T$, where A is estimated as the distance between two adsorbed counterions in the situation when the number of adsorbed counterions is just sufficient to neutralize the macroion, that is $(Q_0/Ze)\pi(A/2)^2 = 4\pi R_0^2$ or $A = 4R_0\sqrt{Ze/Q_0}$. Thus,

$$\Gamma = \frac{(Ze)^{3/2} Q_0^{1/2}}{4\epsilon R_0 T}. \tag{5}$$

In principle, there is also other similar Γ parameters which control correlations between various ions in the bulk; in this work we do not address this aspect.

In the present study, we typically look at the Γ_a values in the range $\Gamma_a = 6-80$. For the estimates, it is useful to keep in mind that Bjerrum length $l_B = e^2/\epsilon T$ is close to 7 Å under typical conditions—at room temperature in water ($\epsilon \approx 80$). In particular, for the typical small ions, for which $a \approx 4$ Å (counting attached water), we get $\Gamma_a \approx 1.7Z$, which is roughly between 4 and 10 for Z between 2 and 7. As regards $\Gamma = \Gamma_a(a/4R_0)\sqrt{ZQ_0/e}$, it may be greater than Γ_a if macroion is strongly charged (Q_0/e is large).

Note also that under typical conditions, such as $m \approx 50 m_H$ and $n_0 \approx (1/10\,\text{Å})^3$, where m_H is proton mass, and n_0 the average density of counterions, the characteristic frequency and time are about $\omega_p \approx 6.6 \times 10^{11}\,\mathrm{s}^{-1}$ and $\omega_p^{-1} \approx 1.5$ ps.

In our molecular dynamics study, the initial positions of coions and counterions are distributed randomly in the domain between the two spheres $R_0 < r < R_M$, each ions having the velocity that satisfies the Maxwell distribution. The integration of the equations of motion is done with the use of the leapfrog method which is equivalent to the Verlet algorithm.[27] The time step of integration is $\Delta t = 0.01\omega_p^{-1}$, and simulation runs are executed up to $5000\omega_p^{-1}$. For the standard run to be mentioned below, it takes about $2.5 \times 10^3 \omega_p^{-1}$ before a state is reached that can be assumed equilibrated, at least in terms of the inverted charge Eq. (9) being stationary. This corresponds to a few nanoseconds for the typical conditions.

Below in Sec. III, we report the simulation results concentrating on the general properties of the charge inversion: its dependence on the radius and charge of a macroion, the valence and density of counterions, and temperature. While changing the parameters, the electrostatic binding energy of counterions to the macroion is kept constant by fixing Γ_Q [Eq. (3)].

In the present study, the following values of parameters are considered ''standard'' and used unless otherwise specified: radius of the macroion $R_0 = 3a$, its charge $Q_0 = -28e$ (assumed negative), valence of the counterions $Z = 7$, and the number of the counterions and coions $N^+ = 52$ and $N^- = 336$, respectively. The radius of the outer boundary sphere is $R_M = 20a$. The temperature is chosen such that $\Gamma_a = 4.2Z$.

To support physical intuition, it is useful to estimate the Debye screening length. Naive application of standard formula yields

$$r_s = \left[\frac{\frac{4}{3}\pi(R_M^3 - R_0^3)\epsilon T}{4\pi e^2(Z^2 N^+ + N^-)}\right]^{1/2} = a\left[\frac{(R_M/a)^3 - (R_0/a)^3}{3\Gamma_a(ZN^+ + Z^{-1}N^-)}\right]^{1/2}, \tag{6}$$

which is about $0.5a$ under the ''standard'' conditions. This result may seem surprising, as physically screening length cannot be smaller than the size of smallest ions.[28] Of course, such a small value of screening length indicates very strong Coulomb interactions in the bulk solution. This fact can also be seen differently, by noting that the parameters controlling validity of the linearized Debye–Hückel theory for the plasma away from macroion are $Z\phi_+^{1/3}\Gamma_a$ and $\phi_-^{1/3}\Gamma_a/Z$, which are both large compared to unity, about 10–200 ($Z = 3-7$) and 1–4, respectively. (These parameters mean the ratio of the Coulomb energy between particles of respective signs and thermal energy at typical distances—controlled by densities.) Thus, we examine the cases under which plasma outside the macroion is very nonlinear. Physically, this is manifested by extensive condensation of coins on multivalent counterions, as will be seen in the results below. Such condensation is analogous to the Bjerrum pairs formation.

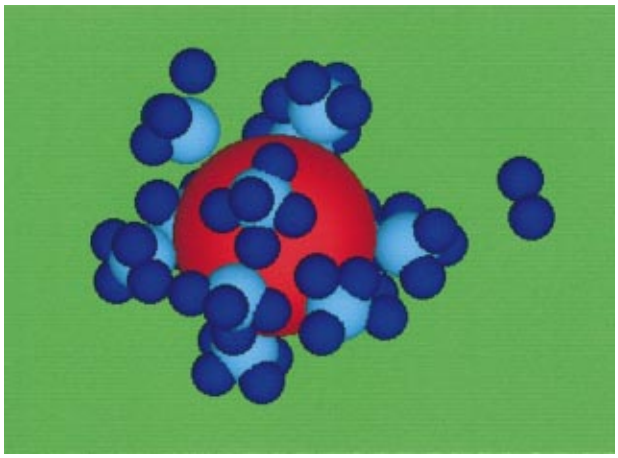

FIG. 1. (Color) The bird's-eye view of the screening atmosphere within $3a$ from the macroion, at $t=5000\omega_p^{-1}$ for the ''standard'' parameters. Macroion is a red sphere in the middle; macroion radius $R_0=3a$ and charge $Q_0=-28e$. Multivalent counterions of valence $Z=7$ and monovalent coions are shown in light blue and dark blue, respectively. Temperature is chosen such that $\Gamma_a=Ze^2/\epsilon aT=29.4$. Note that significant condensation of coions on the counterions is observed. For this reason, correlations between adsorbed multivalent counterions are nowhere near ideal Wigner crystal while $\Gamma\approx 137$ [Eq. (5)] is very large.

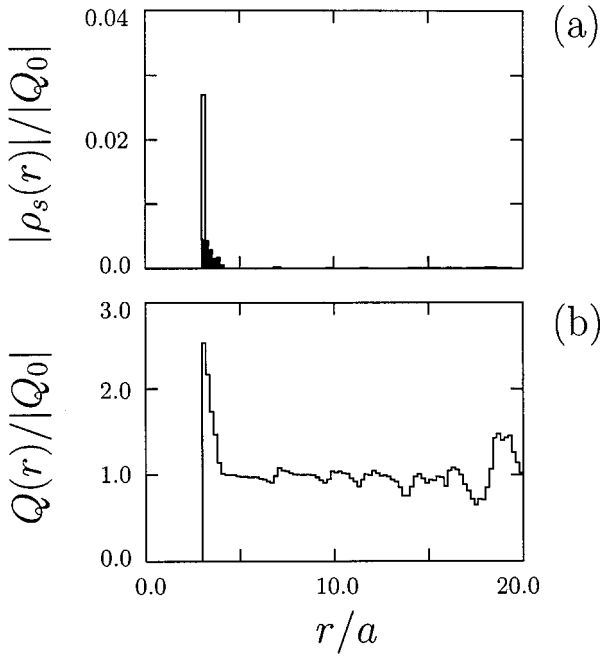

FIG. 2. Charge inversion under the ''standard parameters,'' as in Fig. 1. (a) The radial distribution function of the charge $\rho_s(r)$ [Eq. (8)] of counterions (open bars) and that of coions (shaded bars) as a function of the distance r from the macroion center. (b) The integrated charge distribution $Q(r)$ of counterions plus coions [Eq. (9)]. The portion $Q(r)/|Q_0|>1$ corresponds to charge inversion. Comparatively large fluctuations near the wall is mainly due to the volume element $4\pi r^2$.

Condensation means that effective charges of particles are reduced, and also the effective density of charged particles is lowered. That leads to the increase of real screening radius which attains some respectable value. We do not attempt to estimate it, as we do not rely on any particular theory. Instead, we will just see what molecular dynamics show. We shall see that condensation of coions is the major factor limiting the extent of charge inversion.

Another interesting quantity to estimate is the Gouy–Chapman length associated with the planar surface of a macroion,

$$\lambda=\frac{\epsilon T}{2Z\pi e\sigma}=a\frac{2(R_0/a)^2}{\Gamma_a|Q_0/e|}, \tag{7}$$

where $\sigma=|Q_0|/4\pi R_0^2$, which turns out to be about $0.15a/Z$. (Strictly speaking, λ is defined for the plane, not spherical surface; however, since $\lambda/R_0\approx 0.05\ll 1$, defining λ based on the plane geometry is reasonable.)

III. SIMULATION RESULTS

A. Observing charge inversion

1. Standard regime

The results of our simulations are presented in Figs. 1–9. Figures 1 and 2 present typical results of the run performed under the ''standard'' conditions. Specifically, Fig. 1 shows a snapshot of the spatial distribution of counterions and coions around the macroion after charge distribution has become stationary. Since our simulation includes hundreds of particles, it is impossible to ''see'' all of them in any meaningful way; we show, however, the configuration of ions in the immediate vicinity of the macroion surface, in which only the ions residing in the thin layer $R_0\leqslant r\leqslant R_0+3a$ are depicted.

As seen in Fig. 1, counterions (light blue) attach right on the surface of the macroion with a lateral spacing, while coions (dark blue) stay some distance away from the macroion surface. It is clear that lateral correlations are present between counterions, particularly because there are no pairs in which counterions are close to each other. Not surprisingly, however, these correlations are much weaker than in

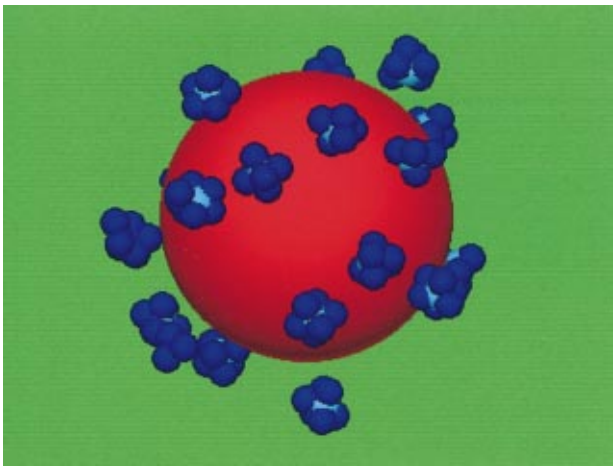

FIG. 3. (Color) The bird's-eye view of the screening atmosphere within $3a$ from a ''large'' macroion, at $t=4000\omega_p^{-1}$ for the run of the macroion radius $R_0=8a$. Other simulation parameters are the same as those of Fig. 1, except that the temperature is adjusted to keep the quantity $Ze^2/\epsilon R_0T$ the same as in Fig. 1. It means that Γ, Eq. (5), is the same here and in Fig. 1, while Γ_a is greater here by a factor of 8/3 than in Fig. 1. Accordingly, stronger binding of monovalent coions (dark blue) to multivalent counterions (light blue) is observed, and adsorbed counterions are less strongly correlated.

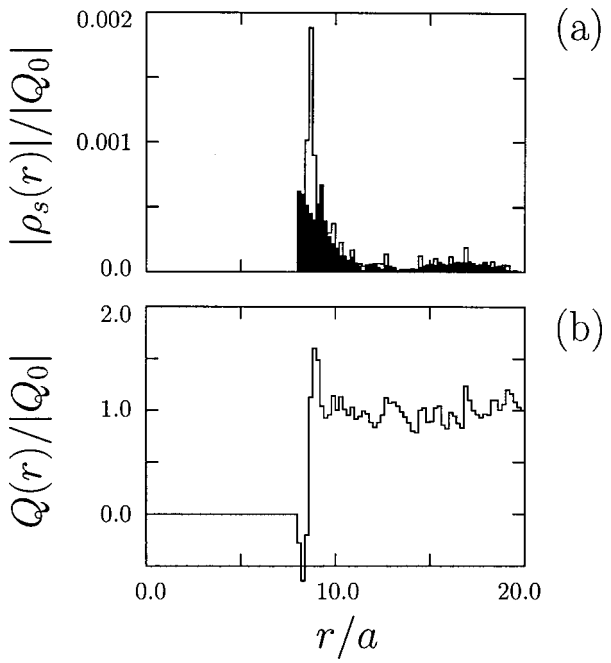

FIG. 4. Charge inversion of a ''large macroion''—the system shown in Fig. 3. Plot format and notations are the same as in Fig. 2. Counterions are loosely bound to the macroion for the reason noted in Fig. 3. Although the amount of inverted charge is smaller compared to that in Fig. 2, it is still significant.

the case without coions examined in the previous work:[20] although counterions are correlated in Fig. 1, their spacings are not regular and cannot be identified as a Wigner crystal. Regarding coions, they are seen to condense on the top side of the counterions, presumably because of strong repulsion of the coions from macroion surface. We note here that this condensation of coions on the counterions is responsible for limiting the amount of charge inversion. In the configuration shown in Fig. 1, the numbers of counterions and coions within the distance a from the macroion surface are $N_a^+ = 11$ and $N_a^- = 5$, respectively. This means that the maximum

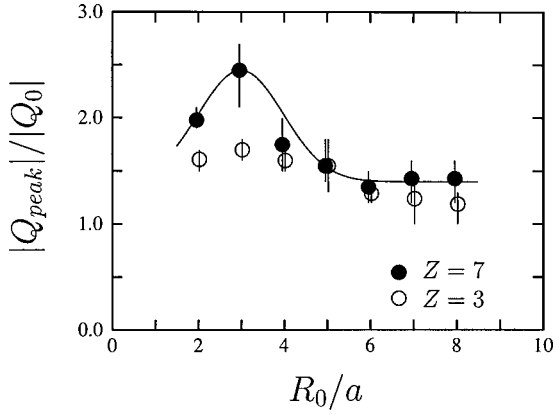

FIG. 5. Dependence of the inverted charge on the radius of macroion R_0 is shown for the counterions with the valence $Z=3$ and 7. The charge of the macroion is $Q_0 = -28e$; the number of coions $N^- = 335$ (or 336) corresponds to the density $n^- \sim 1 \times 10^{-2} a^{-3}$. The ordinate is the maximum of the integrated charge $Q_{\text{peak}} = \max(Q(r))$ [Eq. (9)], normalized by the macroion charge $|Q_0|$. Each data point is an average of three runs, and a vertical bar shows the range of time variations and deviations among the runs.

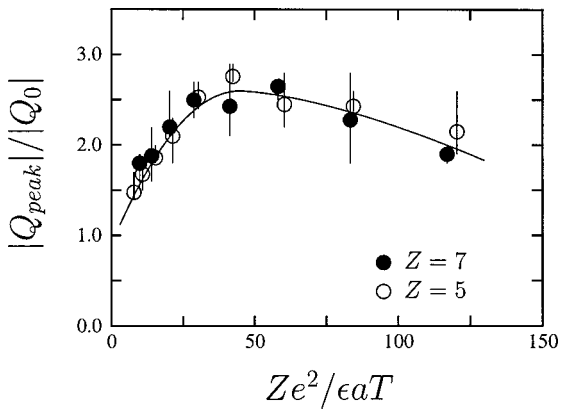

FIG. 6. Dependence of inverted charge on temperature is shown for counterions of different valence Z; it is given by a master curve. The abscissa is the ratio of the Coulomb energy of the counterions to thermal energy, $\Gamma_a = Ze^2/\epsilon aT$. The radius of macroion is $R_0 = 3a$, and the number of coions is kept nearly the same, $N^- \sim 335$ and 336 for $Z=5$ and 7, respectively.

amount of inverted charge, i.e., ''macroion+attached counterion+attached coions,'' is $+44e$. This is to be compared with the bare macroion charge of $-28e$, which amounts to the maximum charge inversion of about 160% the original macroion charge. On the other hand, the net charge of the macroion complex, to which coions and counterions at $r \leqslant R_0 + 2a$ contribute, is roughly $11Ze - 45e + Q_0 \approx +4e$.

Figure 2(a) shows the radial distributions of coion and counterion charges

$$\rho_s(r) = eZ_s \int \sum_{i \in s} \frac{\delta(\mathbf{r} - \mathbf{r}_{si})}{4\pi r_{si}^2} d\Omega_{\mathbf{r}}, \tag{8}$$

where s means either coions or counterions, Z_s is, accordingly, either -1 or Z; summation runs over all ions of the given sort s, $\mathbf{r}_{si}$ is the position vector of ion i of the sort s, and $\Omega_{\mathbf{r}}$ is the solid angle of directions of vector $\mathbf{r}$. Data points of Fig. 2 (and also Fig. 4) are obtained by time averaging to reduce the fluctuations due to finite number and δ-functionlike profile of particles (the bin width is $0.2a$). These results are consistent with the maximum

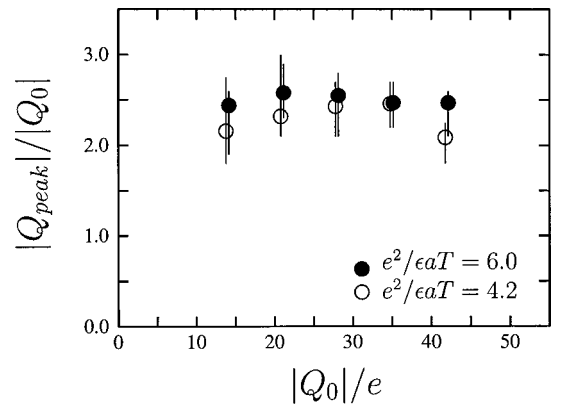

FIG. 7. Dependence of inverted charge on the macroion charge Q_0. The radius of macroion is $R_0 = 3a$, and the valence of counterions is $Z=7$. Temperature is adjusted to keep the binding energy $\Gamma_Q = Ze|Q_0|/\epsilon R_0 T$ constant as Q_0 varies.

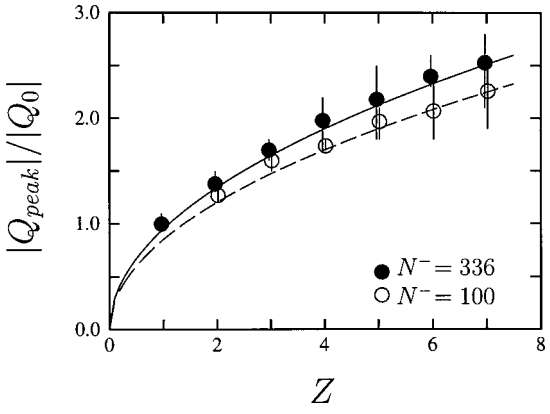

FIG. 8. Amount of inverted charge Q_{peak} increases monotonically with the valence of counterions Z, where temperature is fixed as $e^2/\epsilon aT=4.2$. The inverted charge is well fit by $Q_{\text{peak}}\sim Z^{1/2}$ for $Z\leqslant 5$, and $Q_{\text{peak}}\sim Z$ for $Z>5$. Note that charge inversion occurs only for multivalent counterions, i.e., $Z\geqslant 2$.

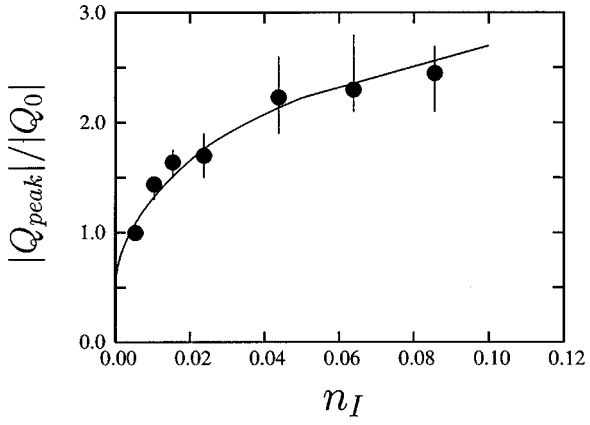

FIG. 9. Dependence of inverted charge on the ionic strength $n_I=(Z^2N^+ +N^-)/V$, where V is the volume of the simulation domain. Charge neutrality of the system is maintained. The guide curve is $n_I^{1/2}$ for $n_I<0.02/a^3$, and n_I for $n_I>0.05/a^3$. The macroion radius is $R_0=3a$, charge $Q_0=-28e$, the valence of counterions $Z=7$, and $\Gamma_a=4.2Z=29.4$.

amount of 160% charge inversion. Indeed, the distribution of the counterions, denoted by open bars, is sharply peaked at $r\cong R_0$, while that of the coions (shaded bars) is broad and detached from the macroion surface. Although at this stage we do not formulate any rigorous algorithmic definition as to which counterions are close enough to the macroion to be called ''bound,'' we note that the peak in the radial density distribution of counterions is sharp enough to provide for quite clear distinction between bound and unbound ions. We therefore rely on this sharp peak, and in what follows we describe as bound those counterions that belong to this peak.

Figure 2(b) depicts the integrated charge of the movable ion species (counterions and coions) of Fig. 2(a), starting at the surface of the macroion,

$$Q(r)=\sum_s \int_{R_0}^{r} \rho_s(r')\,4\pi r'^2\,dr'. \tag{9}$$

The portion above the baseline $Q/|Q_0|=1$ corresponds to the charge inversion (this applies to all the following figures). The maximum amount of inverted charge reaches 160% for this run, as stated above, and the $Q(r)$ profile relaxes to neutrality in a distance of approximately $\approx 2a$, thus suggesting once again that a significant population of coions reside on the outer sides of condensed counterions. Small periodic peaks of $Q(r)$ for $r\gg R_0$ reflect spatially correlated density fluctuations which are much amplified because of the volume factor $4\pi r^2$. On the other hand, we observe a nearly neutral region $Q/|Q_0|\approx 1$ extending for the distance comparable to the Bjerrum length l_B outside the charge inversion layer. Few ions exist in this region. This shows establishment of enhanced order due to strong Coulomb interactions.

The electrostatic potential drop across the charge distribution peak corresponds to energy change $e\Delta\varphi\approx 1.2e^2/\epsilon a$, which is five times the thermal energy k_BT. This implies strong binding of counterions to the macroion and coions to the counterions. In other words, this very strongly manifests nonlinear screening compared with Debye–Hückel screening of weakly coupled cases. Of course, this is by no means surprising given the small value of λ Eq. (7), as mentioned above.

Speaking about the dynamics of equilibration, it is interesting to note that the initial buildup of counterions on the macroion occurs fairly quickly, in about $50-80\omega_p^{-1}$, which is roughly 100 ps for the typical numerical values of parameters, as stated in Sec. II B. This time is much shorter than overall relaxation time of the system $(1\sim 2)\times 10^3\omega_p^{-1}$ (a few ns), suggesting that equilibration of plasma apart from the macroion occurs fairly slowly. It is appealing to guess that this fast buildup of screening (and even overcharging) layer is connected with the strongly nonlinear correlated screening.

2. Other regimes

The charge inversion for the macroion with a large radius $R_0=8a$ is depicted in Figs. 3 and 4. Other parameters are the same as those of Fig. 1, except for the lower temperature ($\Gamma_a=78.4$) to keep $\Gamma_Q=\text{const}$, Eq. (3). We again observe sparsely distributed counterions on the macroion surface. In this case, however, binding of the counterions to the macroion is loose, and their radial distribution in Fig. 4(a) is almost as broad as that of the coions. The counterion charge is better canceled on each site by the condensed coions than in Fig. 1.

We note that the number of condensed ions to the macroion surface in Fig. 3 is $N_{3a}^+\sim 13$ and $N_{3a}^-\sim 66$; the number of N^+ is comparable to that in Fig. 1. This is consistent with the fact that each counterion occupies roughly a neutralizing region on the macroion surface, similar to the Wigner–Seitz cell of Wigner crystal. With surface charge density of the macroion $\sigma=Q_0/4\pi R_0^2$, the size of such neutralizing region, or cell, is proportional to the size of the macroion: $eZ=\pi\sigma R_{ws}^2$, or $R_{ws}=2R_0(Ze/|Q_0|)^{1/2}$. In other words, the neutralizing number of counterions $(R_0/R_{ws})^2$ stays unchanged as long as the macroion charge Q_0 is fixed. The maximum inverted charge in Fig. 4(b) is about 40% the original charge of the macroion, which is less than that in

Fig. 2. The electrostatic potential drop across the macroion surface is consistently less than the thermal energy, $e\Delta\varphi \sim 0.05e^2/\epsilon a < k_B T \sim 0.09e^2/\epsilon a$. The linear Debye–Hückel theory nearly applies in this case.

We find similar features, based on identification of bound ions in the peak of their radial distribution, also for the parameters further away from our standard conditions. For instance, we mention in passing the case of the counterions with smaller valence $Z=3$. For them, it takes somewhat less than $1\times 10^3 \omega_p^{-1}$ to reach the stationary state, and the attained peak height is lower, about 70% the macroion charge, as shown in Fig. 8. This will be discussed in greater details in one of the sections below.

B. Changing macroion properties and temperature

In the following figures, Figs. 5–9, the ordinate Q_{peak} is the maximum of the integrated charge of the counterions plus coions, Eq. (9). Each data point is an average of time and three runs, where a vertical bar shows the range of time variations and deviations among the runs.

The dependence of charge inversion on the radius of the macroion is depicted in Fig. 5. For different values of the radius, temperature is adjusted accordingly to keep unchanged the value of $\Gamma_Q \propto 1/(R_0 T)$, Eq. (3). The valence of the counterions is either $Z=3$ or 7. The number of counterions is $N^+=121$ and $N^+=52$ for $Z=3$ and 7, respectively, which is large compared to $|Q_0|/Ze$ required for charge neutralization of the macroion. These parameters are chosen in such a way that the number of coions, which is determined by neutrality condition, is virtually fixed, being $N^-=335$ for the $Z=3$ case and $N^-=336$ for the $Z=7$ case. This corresponds to r_s, Eq. (6), moderately changing between $0.3a-0.8a$, and λ, Eq. (7), changing between $0.02a-2.8a$.

In Fig. 5, the inverted charge reaches its maximum for the radius $R_0 \approx 3a$ irrespectively of the valence Z. It falls off rapidly both for smaller and larger radii, and becomes insensitive to the radius of the macroion for $R_0/a \gg 1$. The maximum amount of the inverted charge is about 70% of the bare macroion charge Q_0 for $Z=3$; it increases up to 150% of Q_0 for $Z=7$. We find that the charge inversion reaches maximum also at virtually the same radius $R_0 \approx 3a$ even for the smaller number of counterions $N^+=15$ $(Z=7)$, or for larger macroion charge $Q_0=-42e$.

It is not difficult to understand qualitatively why the charge inversion decreases at both small and large values of macroion radius R_0, reaching a maximum in between. When R_0 gets very large, the lateral spacings between bound counterions become too large to maintain correlations between them; on the other hand, when R_0 gets too small, the increased repulsion among the adsorbed counterions becomes dominant.

The effect of temperature on charge inversion is shown in Fig. 6. In this figure, the abscissa is $\Gamma_a = Ze^2/\epsilon a T$ [Eq. (4)]. As the figure indicates, the inverted charge for different values of valence form a master curve when plotted against Γ_a. The charge inversion is maximized at the intermediate temperature corresponding to $\Gamma_a \sim 45$, or $Ze^2/\epsilon R_0 T \sim 15$ $(R_0=3a)$. The value of the Debye length is $r_s \approx 0.6a$ for $Z=3$ and $r_s \approx a$ for $Z=7$. For the low temperature side, $\Gamma_a \sim 100$, the integrated charge distribution $Q(r)$ is sharply peaked as that of Fig. 2(b), while at the high temperature side, $\Gamma_a \sim 10$, the distribution $Q(r)$ is rugged and fluctuates with time. The potential energy between the counterions and macroion decreases remarkably with Γ_a for small Γ_a, and is minimized at $\Gamma_a \sim 40-50$. These observations are consistent with maximal charge inversion achieved through competition of counterion condensation to the macroion and the coion–counterion pairing. Lower temperatures are favored for the former due to larger Coulomb binding energy, and higher temperatures are better to suppress the latter due to enhanced thermal motion.

Charge inversion is insensitive to the charge content of the macroion Q_0 for fixed value of $\Gamma_Q = ZeQ_0/\epsilon R_0 T$ ($\Gamma_a = 4.2Z$ or $6Z$), as seen by $Q_{\text{peak}}/|Q_0| \sim$ const in Fig. 7. The number of counterions attached to the macroion surface is in the range 8–15 for $|Q_0| = (14-42)e$ and $Z=7$, which is a few times that of the neutralizing number of counterions, $|Q_0|/Ze$.

We note in passing that the geometrical capacity of the surface, controlled by non-Coulomb short range forces is still very far from exhausted, $4\pi R_0^2/\pi a^2 \sim 36$. The regime of (almost) closed packing of the bound spheres on the macroion is examined in the recent work.[29] Interestingly, the *effective* valence of the counterions Z_{eff}, which is the charge of the counterion minus that of the condensed ions, increases with the charge of the macroion; it is $Z_{\text{eff}} \sim 0.25Z$ for $Q_0=-14e$ and is $Z_{\text{eff}} \sim 0.4Z$ for $Q_0=-42e$.

C. Changing counterion properties

The dependence of inverted charge on the valence of the counterions is depicted in Fig. 8. Here, the macroion charge and radius are $Q_0=-28e$ and $R_0=3a$, respectively, and temperature is fixed such that $\Gamma_a/Z = e^2/\epsilon a T = 4.2$. It is emphasized that no charge inversion is observed for monovalent counterions. The amount of the inverted charge Q_{peak} increases with the valence, which is well scaled by $Q_{\text{peak}} \sim Z^{1/2}$ for $Z \leqslant 5$. The $Z>5$ part can be fit by $Q_{\text{peak}} \sim Z$. The inverted charge is also an increasing function of the number of counterions and coions, as seen by the difference of the two curves for two densities in the figure.

The dependence of inverted charge on the ionic strength, $n_I = (Z^2 N^+ + N^-)/V$, is shown in Fig. 9, where $V = 4\pi(R_M^3 - R_0^3)/3$ is the domain volume. The amount of inverted charge $Q_{\text{peak}}/|Q_0|$ starts at $(Ze/|Q_0|)^{1/2}$ and increases monotonically with the ionic strength. The functional form of the scaling changes at $n_I \sim 0.05/a^3$, as shown by fitting curves. The ionic strength of a Ca^{2+} ion and neutralizing coions in every 10 Å cube yields $0.048/a^3$ for $a=2$ Å. The scaling $Q_{\text{peak}} \sim n_I^{1/2}$ for the low ionic strength $n_I < 0.02/a^3$ smoothly joins a linear scaling $Q_{\text{peak}} \sim n_I$ for the high ionic strength $n_I > 0.05/a^3$. The nondimensional parameter of the theory,[3] $\zeta = (R_{ws}/r_s)^2 = 12a\Gamma_a N_{ci}(e/|Q_0|)(R_0^2/R_M^3)$, is calculated to be 0.7 for $n_I \sim 0.01/a^3$ and $Z=7$. The theory expects $Q^{(th)} \sim (N_{ci}Z)^{1/2}$ for $\zeta \ll 1$, and $Q^{(th)} \sim N_{ci}Z$ for $\zeta \gg 1$. The present simulation results agree with this theoretical prediction.

IV. CONCLUSION

In this paper, we showed the occurrence of giant charge inversion and its parameter dependences with the use of molecular dynamics simulations. The giant charge inversion occurred in a few nanosecond, which was based on the strong correlations among the multivalent counterions and coexisting coions, particularly on the surface of the macroion. Specifically, charge inversion was observed under the conditions such that the Coulomb coupling parameter was significantly larger than unity, $\Gamma \gg 1$. At the same time, it was necessary that the valence of counterions was larger than unity, $Z \geqslant 2$, in the presence of coions. Counterions attached to the surface of the macroion, while monovalent coions condensed on the counterions. This condensation, similar to the Bjerrum pairing, is therefore identified as the factor limiting the amount of charge inversion. The amount of the inverted charge Q_{peak} was maximal at rather small radius of the macroion, and leveled off at large radii if the macroion charge $|Q_0|$ was fixed. The ratio $Q_{\mathrm{peak}}/|Q_0|$ was independent of the macroion charge, that is, the inverted charge scaled linearly with the charge of macroion.

With respect to the valence Z and the ionic strength $n_I = (Z^2 N^+ + N^-)/V$, the amount of inverted charge scaled as $Q \sim (Z n_I)^{1/2}$ for the valence $Z \leqslant 5$ or $n_I \leqslant 0.02/a^3$. As noted in Sec. III C, this ionic strength corresponds to a Ca^{2+} ion in every 10 Å cube. The inverted charge scaled as $Q \sim Z n_I$ for $Z > 5$ or $n_I > 0.05/a^3$. This scaling agreed with the theory of giant charge inversion.[3] The maximum inverted charge of nearly up to 160% the bare charge of the macroion was achieved at the medium temperature $Ze^2/\epsilon R_0 T \sim 15$, due to the competition of multivalent counterion attachment to the macroion and monovalent coion condensation on the counterions; the former was stronger at lower temperatures, and the latter was suppressed at higher temperatures.

In the present study, the macroion was assumed to be immobile. From the application points of view, it might be informative to study the distribution of counterions and coions around a moving macroion under the influence of an applied electric field. The study of such cases is reported in a separate paper. The results indicate that a formed complex of a macroion and counterions drifts along the electric field in the direction implied by the inverted charge, and that charge inversion is not altered until the electric field exceeds a critical value.[25]

ACKNOWLEDGMENTS

The authors are highly grateful to Professor Boris I. Shklovskii whose suggestions helped them to perform the present study. We also thank him for reading the paper and giving valuable comments. Numerical computations were performed with the use of the vpp800/12 supercomputer of the Institute for Space and Astronautical Science, Japan.

[1] P. Debye, and E. Hückel, Phys. Z. **24**, 185 (1923).
[2] B. I. Shklovskii, Phys. Rev. Lett. **82**, 3268 (1999).
[3] T. T. Nguyen, A. Yu. Grosberg, and B. I. Shklovskii, Phys. Rev. Lett. **85**, 1568 (2000); J. Chem. Phys. **113**, 1110 (2000).
[4] K. Luger, A. Mader, R. Richmond, D. Sargent, and T. Richmond, Nature (London) **389**, 251 (1997).
[5] E. Bakeev, M. Yang, I. Shu, A. Zezin, V. Kabanov, A. Lezov, A. Mel'nikov, I. Kolomiets, E. Rjumtsev, and W. MacKnight, Macromolecules **29**, 1320 (1996).
[6] Y. Wang, K. Kimura, Q. Huang, P. L. Dubin, and W. Jaeger, Macromolecules **32**, 7128 (1999).
[7] V. I. Perel and B. I. Shklovskii, Physica A **274**, 446 (1999).
[8] B. I. Shklovskii, Phys. Rev. E **60**, 5802 (1999).
[9] T. T. Nguyen, A. Yu. Grosberg, and B. I. Shklovskii, Proc. Les Houches School on Electrostatic Effects in Soft Matter and Biophysics, 2000; cond-mat/0101103.
[10] I. Rouzina and V. Bloomfield, J. Phys. Chem. **100**, 9977 (1996).
[11] J. F. Joanny, Eur. Phys. J. B **9**, 117 (1999).
[12] T. T. Nguyen and B. I. Shklovskii, Physica A **293**, 324 (2001).
[13] T. T. Nguyen and B. I. Shklovskii, J. Chem. Phys. **114**, 5905 (2001).
[14] A. V. Dobrynin, A. Deshkovski, and M. Rubinstein, Macromolecules **34**, 3421 (2001).
[15] F. J. Solis and M. Olvera de la Cruz, J. Chem. Phys. **112**, 2030 (2000).
[16] R. R. Netz and H. Orland, Eur. Phys. J. E **1**, 203 (2000).
[17] L. Gulbrand, B. Jonsson, H. Innerstrom, and P. Linse, J. Chem. Phys. **80**, 2221 (1984).
[18] L. Sjostrom, T. Akesson, and B. Jonsson, Ber. Bunsenges. Phys. Chem. **100**, 889 (1996).
[19] A. G. Moreira and R. R. Netz, Europhys. Lett. **52**, 705 (2000).
[20] R. Messina, C. Holm, and K. Kremer, Phys. Rev. Lett. **85**, 872 (2000).
[21] R. Messina, C. Holm, and K. Kremer, Europhys. Lett. **51**, 461 (2000).
[22] J. C. Crocker and D. G. Grier, Phys. Rev. Lett. **73**, 352 (1994).
[23] G. M. Kepler and S. Fraden, Phys. Rev. Lett. **73**, 356 (1994).
[24] T. Squires and M. Brenner, Phys. Rev. Lett. **85**, 4976 (2000).
[25] M. Tanaka and A. Yu Grosberg, The 75th Colloid and Surface Science Symposium, 2001.
[26] A. Kornyshev and S. Leikin, Phys. Rev. Lett. **84**, 2537 (2000).
[27] D. Frenkel and B. Smit, *Understanding Molecular Simulation* (Academic, New York, 1996).
[28] To make a bridge to the theoretical work (Ref. 3) we note that screening radius smaller than a was indeed considered there, but that was because multivalent counterions were considered to have the size a, while monovalent coions were considered to have smaller size. Therefore, Debye screening length remained longer than the size of *smallest* ions.
[29] T. Nguyen and B. Shklovskii (private communication).